Analysis of subreflectors for dual reflector antennas

N.C. Albertsen, M.Sc., Ph.D., M.I.E.E., and K. Pontoppidan, M.Sc., Ph.D., Mem.I.E.E.E.

Indexing terms: *Antennas, Optics*

Abstract: The paper presents various methods for the calculation of the field reflected from a subreflector in a dual reflector antenna system. It is demonstrated that the physical-optics (PO) solution agrees well with the geometrical theory of diffraction (GTD) for the copolar component. Significant discrepancies may appear for the crosspolar component, and it is necessary to introduce additional fringe currents in the PO solution. If the subreflector is located in the near field of the feed, special precautions must be taken. One can either subdivide the feed aperture into a number of smaller subapertures for each of which standard GTD can be applied or an alternative and more efficient method is to use complex ray analysis (CRA), where the directive feed is represented by a point source located in the complex co-ordinate space. Both methods are compared with PO solutions taking the near-field effects into account. The theoretical results are verified experimentally for a near-field illuminated offset hyperboloidal subreflector.

1 Introduction

The spacecraft antennas to be developed in the next decade are going to be of increasing complexity. One example is a dual reflector antenna with shaped surfaces and many feeds operating simultaneously. For the analysis of these types of antennas both fast and accurate software must be available.

The geometrical theory of diffraction (GTD) is known to be a very effective tool for reflector antenna analysis. The physical-optics (PO) method is still the only practical solution in the main beam region of a focused reflector, but in the wide-angle sidelobe region GTD is superior to PO, and this is also the case for the determination of subreflector scattered fields. The results obtained with GTD and PO always compare well for the copolar component of the scattered field and the superiority of GTD is therefore more a question of computer time and a clearer interpretation of the calculated pattern. However, for the prediction of low crosspolar components, significant differences of the order of 10–20 dB between GTD and PO have been found. With the present severe requirements to low crosspolar fields for reflector antenna systems designed for frequency re-use this ambiguity is not acceptable. It is important to understand the nature of this difference and this is attempted in the following, where subreflector scattered fields are investigated by means of physical-optics methods, asymptotic methods as well as moment methods.

The material presented here will be based on References 1, 2 and 16. The analysis of reflector antennas in general, and subreflectors in particular, has received so much attention in the literature that an exhaustive bibliography cannot be given here, but some important contributions are listed, namely References 3, 10, 13, 14, 15 and 19.

2 Survey of methods

The methods which will be discussed are:

(*a*) MM—method of moments. The scattering problem is formulated as an E-field integral equation, which is solved by the method of moments [12]. Only applicable to rotationally symmetric reflectors

(*b*) PO—physical optics. The vector potential for the scattered field is generated by surface currents $\boldsymbol{J}^{PO} = 2\hat{\boldsymbol{n}} \times \boldsymbol{H}^i$, where $\hat{\boldsymbol{n}}$ is the surface normal and $\boldsymbol{H}^i$ is the incident field

(*c*) PTD—physical diffraction theory. The vector potential for the diffracted field is generated by surface currents $\boldsymbol{J}^{PTD}$. These are the so-called nonuniform fringe currents [17]. For a curved edge the same expressions as for a straight edge will be used, measuring the distance to the edge along a geodesic

(*d*) GO—geometrical optics. The leading term in an asymptotic expansion of the field reflected from a surface for large values of the wave number k

(*e*) GTD—geometrical theory of diffraction. The leading term in an asymptotic expansion of the field diffracted from an edge. The classical diffraction coefficients were derived by Keller. For practical purposes they are modified according to Reference 9 to correct the results at reflection and shadow boundaries. Furthermore, a caustic correction is included. Unless otherwise specified, the term GTD will be assumed to include GO components in the following

(*f*) APO—asymptotic physical optics. A description of the diffracted field based on the first term of an asymptotic expansion of PO [1]. Whenever APO results are shown in the following, they are corrected at shadow and reflection boundaries and at caustics in exactly the same way as GTD

(*g*) CRA—complex ray analysis. An extension of GTD to rays in complex space co-ordinates.

Traditionally, subreflectors have been synthesised by GO and analysed by PO or GTD. Both the latter methods have limitations, however, and in order to discover these it is convenient to have alternative methods such as MM, although this method can never be an alternative due to its heavy demand on computer storage and CPU time. Similarly, PTD and APO are techniques which are included only to shed light on the discrepancies between PO and GTD. The last method, CRA, may well be the ultimate approach for problems which cannot be handled satisfactorily by PO or GTD. The method has already been studied extensively [4–8, 18], but it is not yet in a form where it can be applied as easily as PO and GTD.

3 Feed models

It is customary to assume that the feed can be considered to be a point source with an angular-dependent radiation pattern. For a balanced feed, therefore, the field can be expressed, in a feed centered co-ordinate system, as

$$\boldsymbol{E}(r, \theta, \phi) = f(\theta)(\sin \phi \hat{\boldsymbol{\theta}} + \cos \phi \hat{\boldsymbol{\phi}}) \frac{e^{ikr}}{kr} \tag{1}$$

Paper 2997H (E11), received 20th October 1983

The authors are with Ticra A/S, Kronprinsensgade 13, DK-1114, Copenhagen K, Denmark

Since the problem is linear there is no restriction in the applicability of the results due to the choice of linear polarisation. The expression in eqn. 1 can only be realised approximately by an actual feed since it only satisfies Maxwell's equations asymptotically for large values of kr. For some of the methods to be discussed eqn. 1 will prove inadequate, since the subreflector is in a region where the field cannot be described by eqn. 1. A correct description of the field may then be obtained through a far field to near field transformation of eqn. 1 via Hansen's spherical vector functions.

Three particular choices of $f(\theta)$ will be used frequently:

$$f(\theta) = 1 \tag{2}$$

$$f(\theta) = 10^{-(\alpha/20)(\theta/\theta_0)^2} \tag{3}$$

$$f(\theta) = \cos^2\left(\frac{\pi\theta}{2\theta_0}\right) \tag{4}$$

Eqn. 2 models an isotropic source. Although of no practical interest, eqn. 2 has the interesting property of a negligible near-field zone, whence eqn. 1 is accurate for all relevant values of kr. The standard feed pattern eqn. 3 models a corrugated feed with a taper of α dB at the angle θ_0. This model is physically most relevant. With eqn. 3 it is no longer possible to use eqn. 1 in the intermediate near field where, in particular, the phase of eqn. 1 becomes inaccurate. The range of kr beyond which eqn. 1 is applicable depends on α and θ_0. Eqn. 4 does not represent a useful physical feed, but is included as an academic model, which has the property that both the far field and its derivative are zero for $\theta = \theta_0$. It is evident that eqn. 4 can only be produced by a very large aperture and therefore eqn. 1 is only applicable for very large values of kr. In Fig. 1 the angular dependences of the amplitude of the magnetic field for eqn. 4 in the far field and for $kr = 44.43$ are shown. Notice the radial component H_r, which is absent in the far field, and the difference in shape of the transverse component H_t. Suppose that the feed illuminates a subreflector placed such that the edge coincides with $\theta = \theta_0$. An uncritical use of eqn. 1 will then produce zero edge illumination and therefore no depolarisation, whereas the true edge field has a finite value, producing a depolarised field which increases as the subreflector is moved closer to the feed. The significance of the difference between eqn. 1 and the correct near field will be illustrated later by PO calculations based on either an incident field given by eqn. 1 or by the correct near field represented by a spherical vector wave expansion.

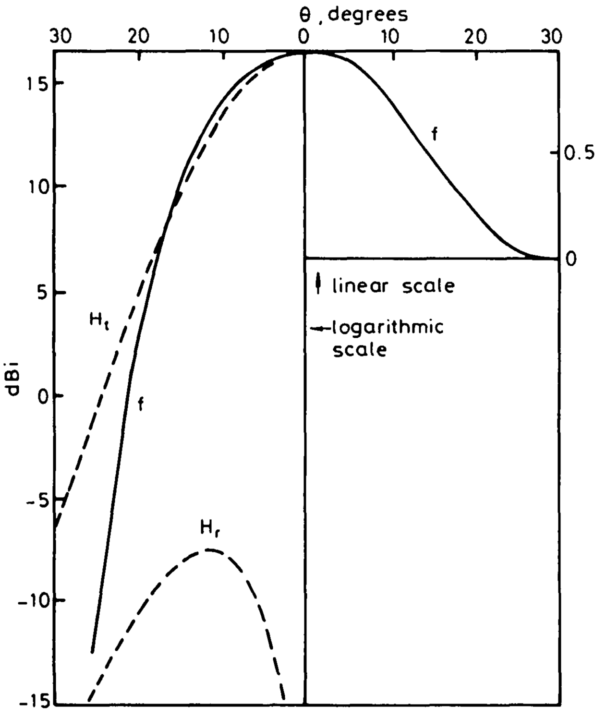

Fig. 1 *Far field and near field at $kr = 44.43$ for feed model (eqn. 4) with $\theta_0 = 28.7°$*

— · — far field
- - - - - near field

4 PO versus GTD

In the physical-optics method it is assumed that the surface current is $2\hat{n} \times \boldsymbol{H}^i$ on the illuminated side and zero on the shadow side. At the edges of the reflector this current is truncated, but, in reality, the edges will give rise to so-called fringe currents in addition to the PO current. These fringe currents are determined from a canonical problem of a plane wave incident on a perfectly conducting halfplane. Let the halfplane lie in the xz-plane with the edge along the z-axis, and let the direction of the incident plane wave be given by the vector $\boldsymbol{k}$. The total current, $\boldsymbol{J}$, then has the following components along x and z:

$$J_x = J_x^{PO} F\left(2\sqrt{\frac{k_t x}{\pi}} \cos\frac{\phi_i}{2}\right) \tag{5}$$

$$J_z = J_z^{PO} F\left(2\sqrt{\frac{k_t x}{\pi}} \cos\frac{\phi_i}{2}\right) + \sqrt{\frac{2i}{\pi k_t x}} \frac{\sin\frac{\phi_i}{2}}{k_y} (k_x J_x^{PO} - k_t J_z^{PO}) \exp i(k_t - k_x)x \tag{6}$$

where J_x^{PO} and J_z^{PO} are the PO components of the current, $F(x)$ is the Fresnel function, k_x, k_y and k_z are the components of $\boldsymbol{k}$, $k_t = \sqrt{k_x^2 + k_y^2}$ and ϕ_i is the angle between the xz-plane and the plane spanned by $\hat{z}$ and $\boldsymbol{k}$. The PTD current is now defined as the difference between the actual current and the PO current, namely

$$\boldsymbol{J}^{PTD} = \boldsymbol{J} - \boldsymbol{J}^{PO} \tag{7}$$

Finally, the vector potential, A, for the scattered field is given by:

$$A = \frac{\mu_0}{4\pi} \iint_S \boldsymbol{J} \frac{e^{ikR}}{R} da \tag{8}$$

where S is the surface, R is the distance between integration point and field point and $\boldsymbol{J}$ may be either of the current contributions defined above.

The properties of PO may be briefly summarised as follows:

(*a*) the method is very time consuming, except in the case of a focused reflector

(*b*) there is no restriction on the complexity of the source pattern

(*c*) the surface currents are slightly in error due to the curvature of the reflector

(*d*) the edge currents are incomplete and PO cannot predict depolarisation unless corrected by PTD.

The limitation in (*a*) could be qualified as follows: the demand on CPU time is proportional to the number of integration patches used in the evaluation of eqn. 8. For a subreflector the patches should not exceed $0.8 \times 0.8\lambda^2$ to obtain a dynamic range of 40 dB. In the following, many of the subreflectors analysed will be rotationally symmetric, and in these cases the symmetry has been exploited to reduce eqn. 8 to a one-dimensional integral. The integration can then be performed with a Romberg scheme and convergence is assured at all pattern levels.

The properties of GTD may be briefly summarised as follows:

(*a*) the method is very fast

(*b*) it is only valid for feeds which can be modelled by a point source

(*c*) the subreflector must be at least 5λ in diameter, unless multiple diffractions are included, and the radius of curvature of the surface must exceed 5λ everywhere.

The first case we shall examine is the rotationally symmetric hyperboloidal reflector shown in Fig. 2. In order to avoid any near-field effects from the feed we use the model eqn. 2. Since the crosspolarisation is of principal interest, all the patterns shown are calculated in a plane bisecting the right angle between *E*- and *H*-planes. In Fig. 3 the amplitude of the copolar beam is shown. All the methods shown agree well, except close to the caustic at $\theta = 0°$, where GTD exhibits slightly larger ripples than the other methods. In Fig. 4 the phase of the copolar pattern is plotted. Good agreement is again found for all methods, except for an almost constant phase difference between MM and the other methods. The reason for this is that the MM solution has not completely converged yet. It was found that from a certain point the amplitude of the MM pattern had converged to within 1/10 dB, whereas increasing the number of unknowns would still affect the phase of the pattern significantly. Fig. 5 finally shows the amplitude of the crosspolar patterns for various methods. As pointed out previously, PO cannot account properly for depolarisation, and Fig. 5 clearly shows that PO predicts a crosspolar field which is far too small compared with GTD and MM. The close agreement between GTD and MM leads us to believe that they show the true level of crosspolarisation. In order to correct PO, the PTD component

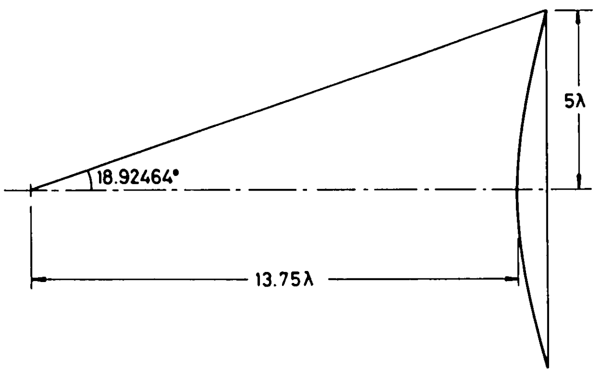

Fig. 2 *Rotationally symmetric subreflector*
Eccentricity of hyperbola $e = 2$
Feed at external focus

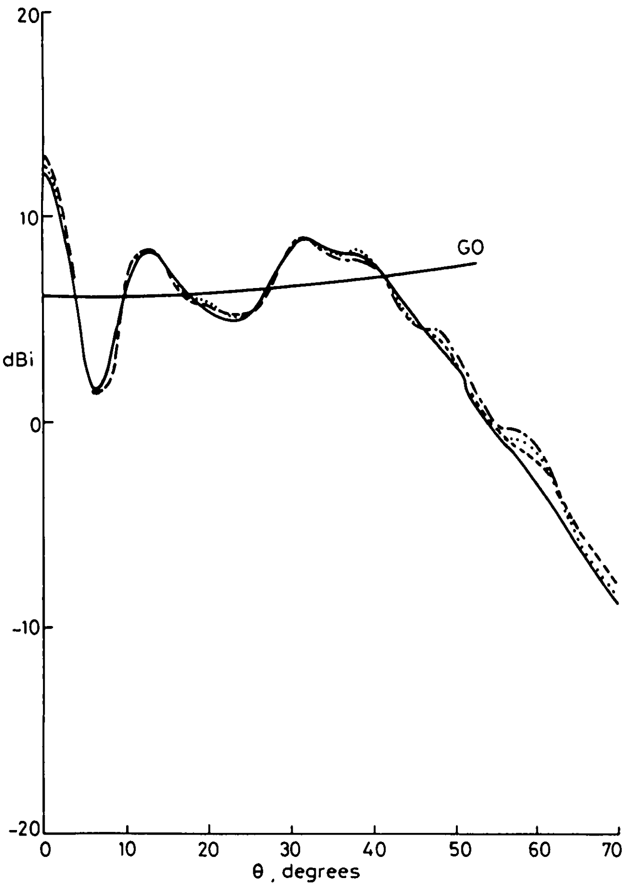

Fig. 3 *Scattered field from subreflector illuminated by isotropic source*
Copolar amplitude
——— PO
— · — GTD
- - - - - PO + PTD
. . . . MM

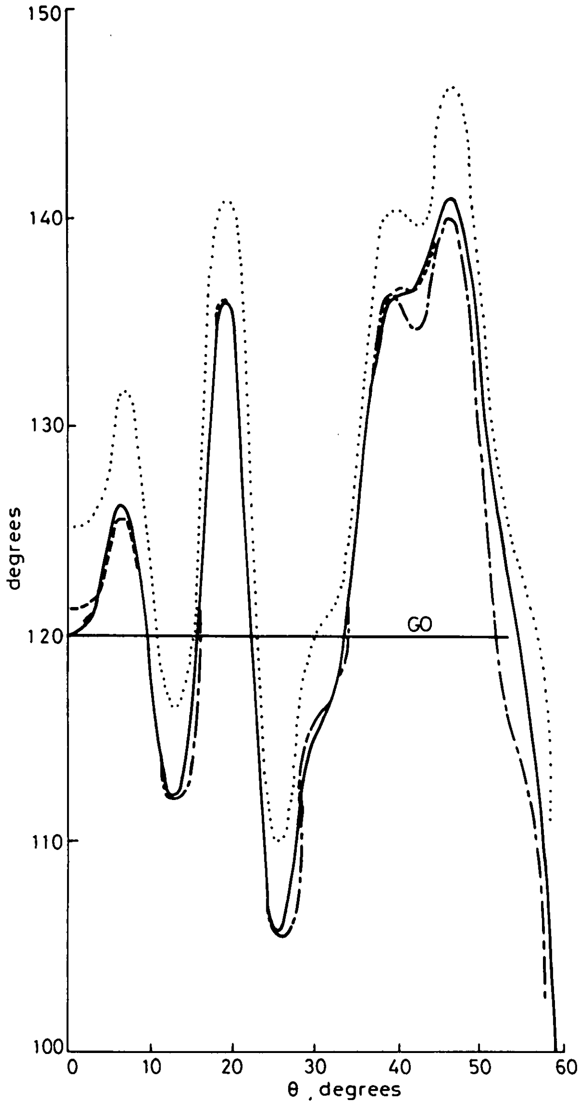

Fig. 4 *Scattered field from subreflector illuminated by isotropic source*
Copolar phase
——— PO
— · — GTD
- - - - - PO + PTD
. . . . MM

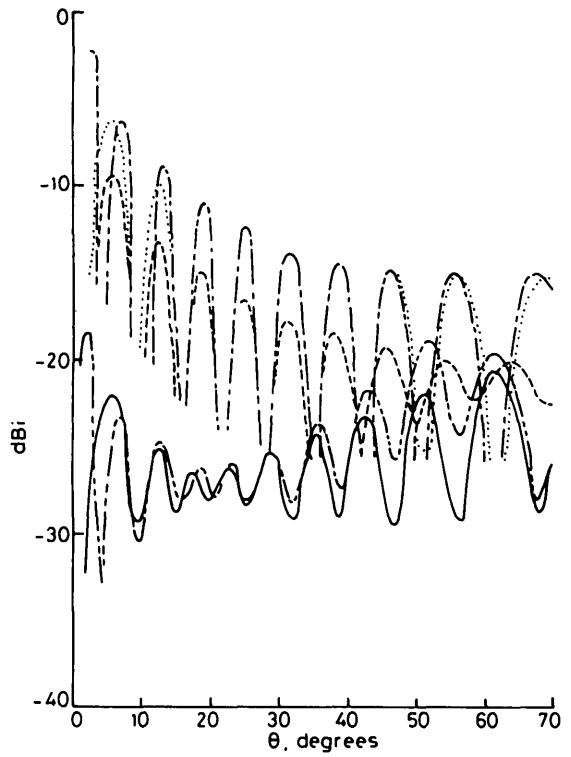

Fig. 5 *Scattered field from subreflector illuminated by isotropic source*
Crosspolar amplitude
- · - · GTD
- -- (c) APO
- —— PO
- - - - - PO + PTD
- .... MM

was added and a much better agreement with MM is now obtained. The remaining difference between PO + PTD and MM is ascribed to the fact that the present structure has a curved edge and the PTD currents will be compressed inside the edge. Finally, an APO solution is also shown. The APO pattern agrees very well with the PO pattern, except close to the caustic, and we conclude that the size and shape of the subreflector are such as to permit the use of asymptotic methods.

The above investigation was repeated for the realistic feed pattern (eqn. 3) with $\alpha = 10$ and $\theta_0 = 18.925°$. In Fig. 6 the amplitude of the copolar beam is shown and good agreement is found for all the methods shown, even close to the caustic since the caustic effects have been decreased by 10 dB relative to Fig. 3. In Fig. 7 the phase of the MM solution is shown for a varying number of unknowns. Even for the best solution shown, the phase has not completely converged, in particular not close to the caustic. Since the beam radiated by the feed is quite narrow with a 10 dB edge taper, eqn. 1 can no longer be used to calculate the incident field at the subreflector. The difference in the incident field at the subreflector when calculated from eqn. 1 compared with the true near field lies almost exclusively in the phase for the geometry considered, and in Fig. 7 the near-field expression was used. In Fig. 8 is shown the phase of the copolar beam using PO; both when the incident field is given by eqn. 1 (labelled far field) and when the near field is used (labelled near field). It is evident that the difference in phase can be very significant. Since the MM solution has not converged completely, we have no absolute reference, but a comparison between Figs. 7 and 8

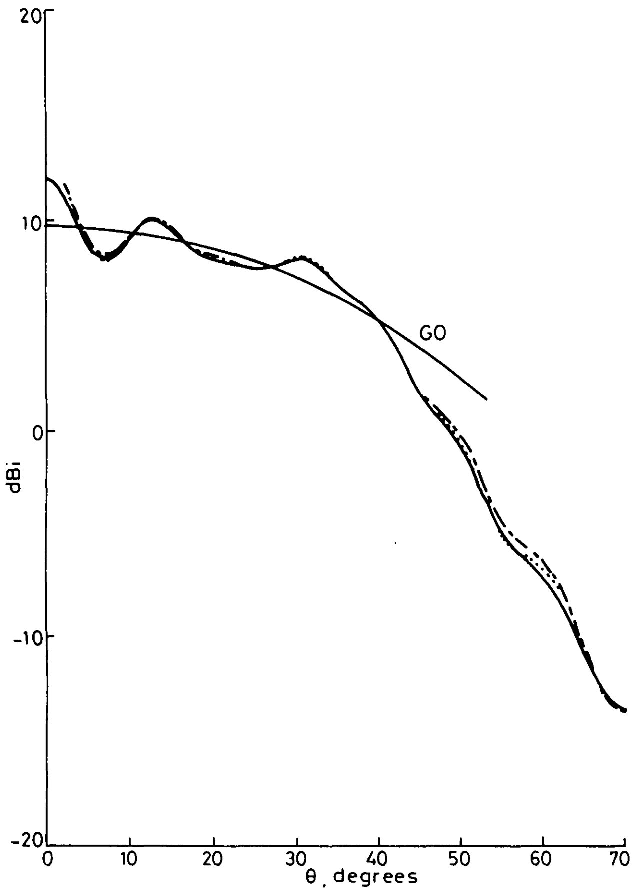

Fig. 6 *Scattered field from subreflector illuminated by feed providing 10 dB edge taper*
Copolar amplitude
- ——— PO, near field
- · - GTD
- .... MM

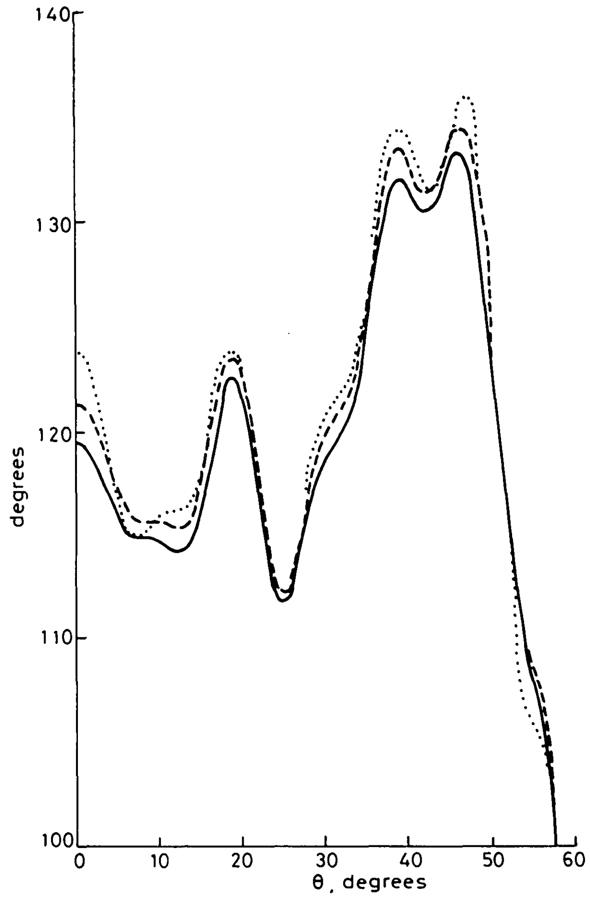

Fig. 7 *Scattered field from subreflector illuminated by feed providing 10 dB edge taper*
Convergence of MM copolar phase
- ——— MM, 98 rings
- - - - - MM, 68 rings
- .... MM, 52 rings

shows that the curve labelled near field in the latter case is probably close to the true phase curve.

Consider now the curve in Fig. 8 calculated by GTD. The method requires that the field can be described as rays

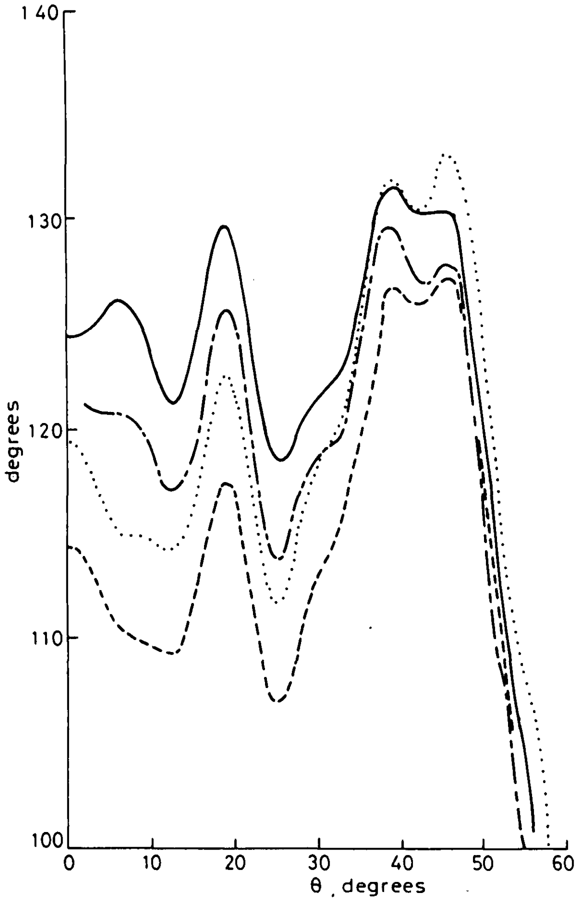

Fig. 8 *Scattered field from subreflector illuminated by feed providing 10 dB edge taper*

Copolar phase
— PO, far field
- - - - - PO, near field
— - - GO + GTD
.... MM

and it is necessary to use eqn. 1 to represent the feed. This does not, however, have the same disastrous effect on GTD as on PO. To understand this, consider reflection in an infinite plane placed in the near field of the feed. The reflected field can be found exactly by image theory and obviously GO will describe the reflected field accurately. On the other hand, PO requires that the currents on the plane are calculated and the phase error introduced here will remain in the reradiated field. In the present case the reflector is not plane, and the field includes edge diffracted rays, whence it must be expected that the near-field effect will also be present in GTD, although less pronounced than in PO. Fig. 8 shows that this is indeed the case. Finally, Fig. 9 shows the amplitude of the crosspolar component. The agreement between the MM solution and the GTD solution is here, as in Fig. 5, very good, whereas PO again predicts a crosspolar level which is far too low (the PO solution plotted is 'far-field'; PO 'near-field' deviates less than 1 dB everywhere).

To illustrate the importance of using the correct near field from the feed in PO, a calculation with the feed model (eqn. 4) was made for a convex, spherical subreflector with the edge at $\theta = 28.68^\circ$ and a diameter of 10λ. Fig. 10 shows the co- and crosspolar patterns with PO (using eqn. 1) and APO and good agreement is found. If, however, the radial component, H_r, of the incident field is included in APO, the crosspolar field decreases by 30 dB. In Fig. 11 the correct near field from the feed is used, and results are shown where only the transverse component, H_t, is used

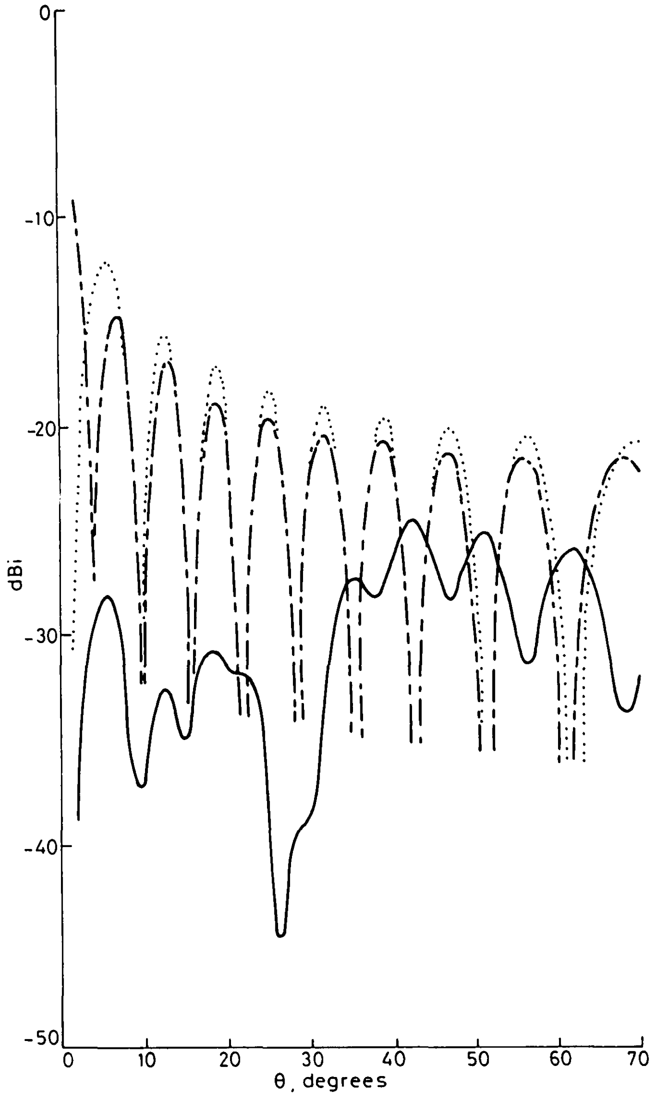

Fig. 9 *Scattered field from subreflector illuminated by feed providing 10 dB edge taper*

Crosspolar amplitude
— PO
— - — GTD
.... MM

and where the total incident H-field is used. It is thus evident that neglect of near-field effects of the feed may lead to an overestimation of the crosspolar field in PO, as well as to a phase error in the copolar field. Finally, Fig. 11 shows that PTD adds approximately 10 dB to the crosspolar field. It should be noted that the erroneous crosspolar component in Fig. 10 has a slow phase variation, which would make it reappear in the secondary pattern, whereas the crosspolar lobes in the PO + PTD result in Fig. 11 have a 180° phase shift from lobe to lobe.

5 GTD versus CRA

It has now been shown that when the subreflector is in the near-field range of the feed, GTD based on eqn. 1 is no longer applicable. The alternative, to use PO with a near-field expansion of the feed and correcting with PTD, is highly inefficient, and it is necessary to search for a corrected GTD approach. One possibility is to split the feed into a cluster of point sources [11]. This has been tried for a geometry very similar to that in Fig. 2, only the semi-apex angle was 17°, the ellipticity of the hyperboloid was

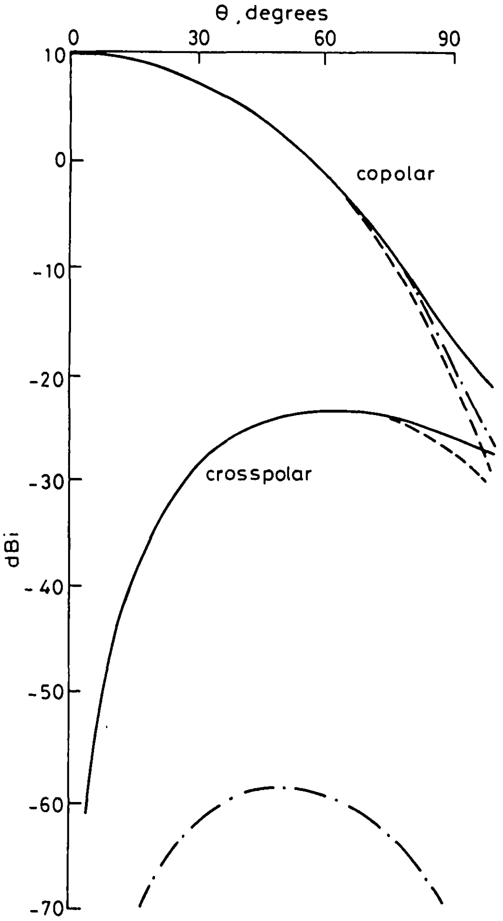

Fig. 10 *Feed model (eqn. 4) illuminating spherical subreflector*
——— PO, far field
- - - - - APO
- · - · - · APO including H_r

1.67 and the distance from the feed to the subreflector 13.19λ. The feed model is eqn. 3 with $\alpha = 15$ and $\theta_0 = 17°$, corresponding to a corrugated feed with an aperture diameter of about 4.8λ and semi-apex angle 9.5°. The feed aperture was split up into nine overlapping subapertures by applying suitable weight functions to the aperture field. Fig. 12 shows the contour lines of the weight functions, each shadowed area being a maximum for one function. The radiation from each subaperture is then represented as coming from a point source. Since these point sources are different in both radiation pattern and orientation, the procedure is cumbersome. The results obtained with nine sources are labelled GTD-9 in contrast to the results obtained with one source labelled GTD-1.

A much more efficient way to model the feed in the near field is the complex source point model used in CRA. The field from a point source:

$$u = \frac{e^{ikR}}{kR}$$
$$R = \sqrt{\rho^2 + z^2 - b^2 - i2bz} \tag{9}$$
$$\rho^2 = x^2 + y^2$$

where R, the distance from the source to the field point, represents, for $R \neq 0$, an exact solution to Helmholtz's equation for an isotropic source in the complex point (0, 0, ib). Since R is complex, it is important to define the proper branch cuts. We shall choose the branch cuts which make the real part of R positive to obtain a field travelling away from the origin in all directions on the far-field sphere. For $z = 0$ we have $R = -i\sqrt{b^2 - \rho^2}$ and the field distribution

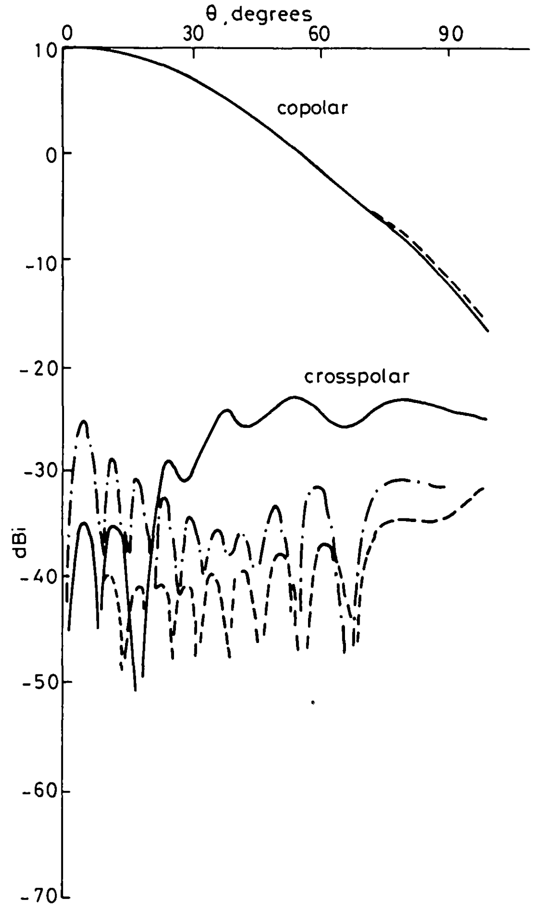

Fig. 11 *Feed model (eqn. 4) illuminating spherical subreflector*
——— PO, near field, only H_t
- - - - - PO, near field, total H
- · - · - · PO, near field, total H + PTD

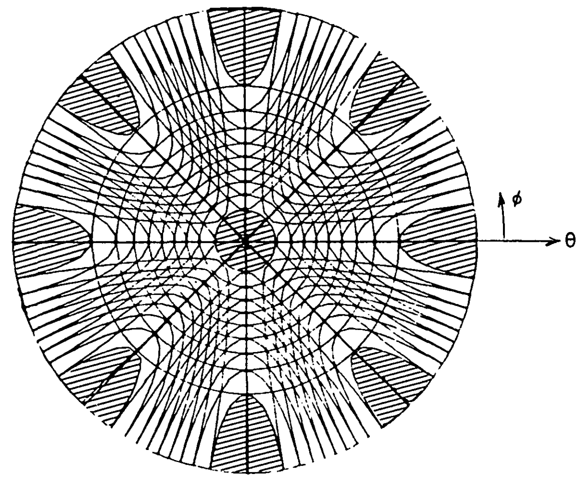

Fig. 12 *Contour lines for weight functions*

here is shown in Fig. 13 for different values of b. In the far field an asymptotic expansion of R gives

$$u = e^{kb\cos\theta}\frac{e^{ikr}}{kr} \tag{10}$$

To model a balanced feed as eqn. 3 the scalar model (eqn. 9) is adequate, since the vector nature of the field is as in eqn. 1 in both the near field and the far field. For feeds with different E- and H-planes and/or pronounced sidelobes, more complicated models involving several complex sources are needed. Figs. 14 and 15 show a comparison between the field from the above mentioned corrugated

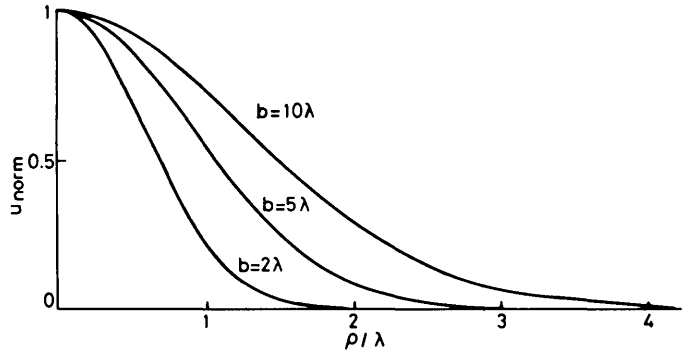

Fig. 13 *Complex source field in aperture plane*

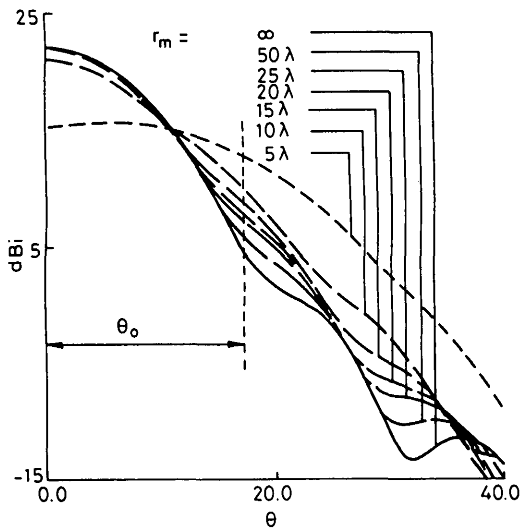

Fig. 14 *Field from corrugated feed*

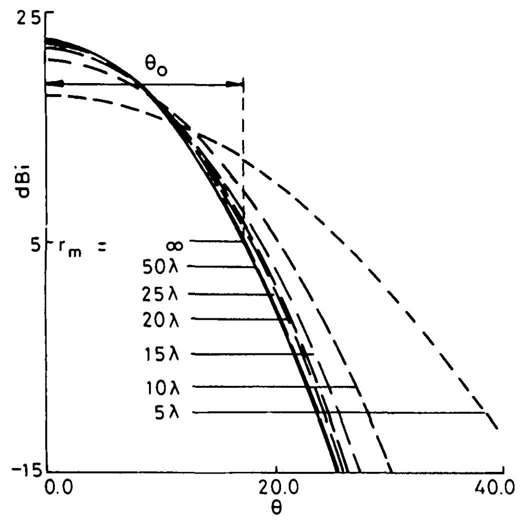

Fig. 15 *Field from complex source*

feed and the field from a complex source point on spheres of increasing radius, and remarkably good agreement is observed in the angular range of interest. Since the field originates from a complex point, it must travel along rays in complex space to reach the real field points of physical interest. This means that also the reflection point on the reflector surface will, in general, be located in the complex space, and it therefore becomes necessary to make an analytical continuation of the surface into complex coordinates. This is a simple matter when the surface is given by an analytical expression [18], and it turns out to be possible also when the surface is tabulated. The calculation of the reflected field takes place as for a real source point, but the caustic distances will be complex. Also, the edge diffracted rays must be included in CRA. The diffraction coefficients in Reference 9 have been generalised to complex angles [2], and the only new problem facing the user of CRA is the definition of the shadow boundary, since the reflection point lies on the complex continuation of the surface and therefore never crosses the reflector edge in real space. The answer is found from the solution of the halfplane problem [6] and involves a combination of the real and imaginary parts of the angle between the incident ray and the surface.

Fig. 16 shows a comparison of the results of GTD-1 and GTD-9, and the most significant difference lies in the copolar beam, where both amplitude and phase differ. In order to check GTD-9, Fig. 17 shows a comparison

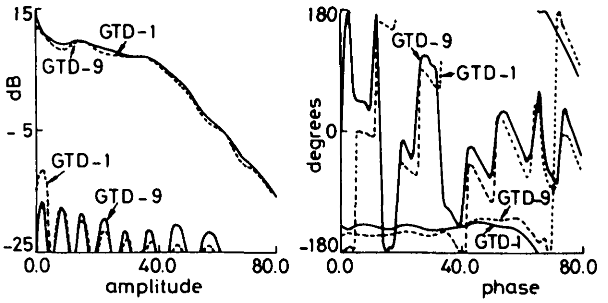

Fig. 16 *Scattered field from subreflector*
Comparison between GTD-1 and GTD-9

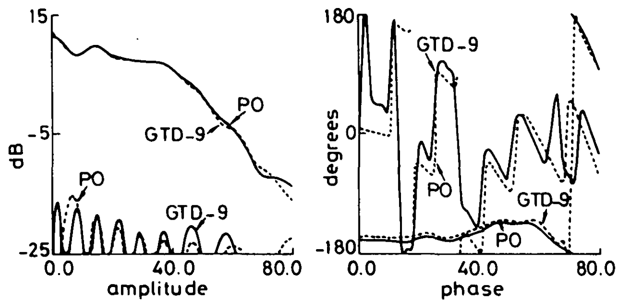

Fig. 17 *Scattered field from subreflector*
Comparison between GTD-9 and PO

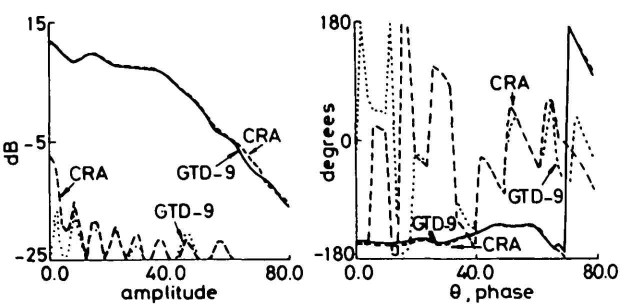

Fig. 18 *Scattered field from subreflector*
Comparison between GTD-9 and CRA

between GTD-9 and PO (using the feed near-field and PTD corrections) and both amplitude and phase of the copolar beam agree very well. Finally, in Fig. 18, GTD-9 has been compared with CRA and again very good agreement is found, in this case also for the crosspolar field (except close to the caustic at $\theta = 0°$).

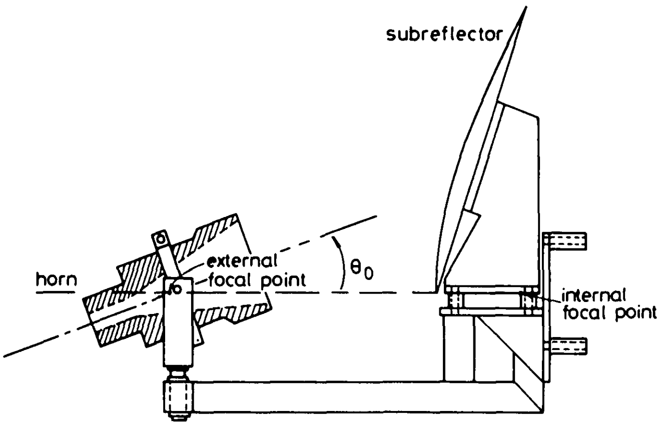

Fig. 19 *Antenna setup*

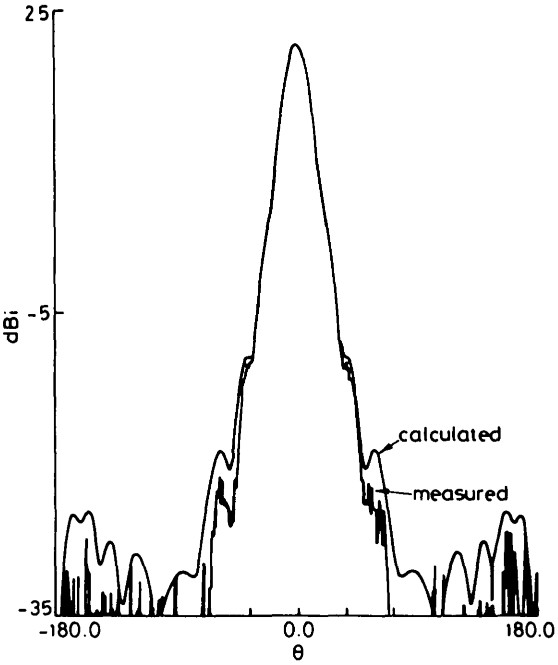

Fig. 20 *Feed amplitude pattern*
H-plane

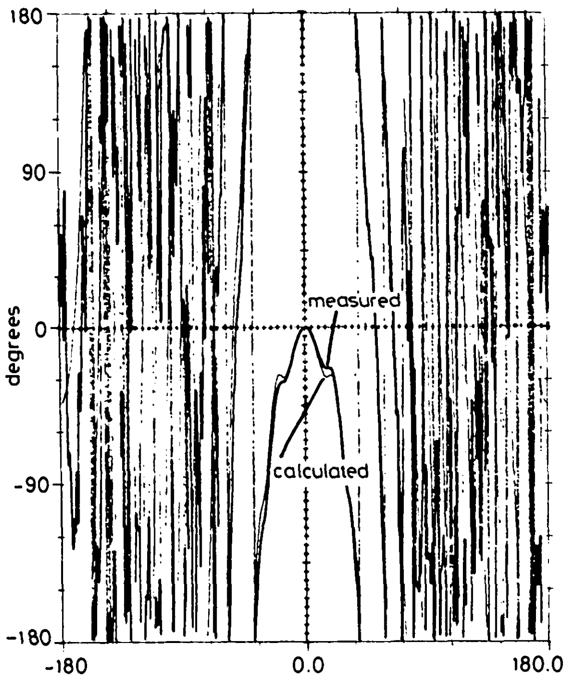

Fig. 21 *Feed phase pattern*
H-plane

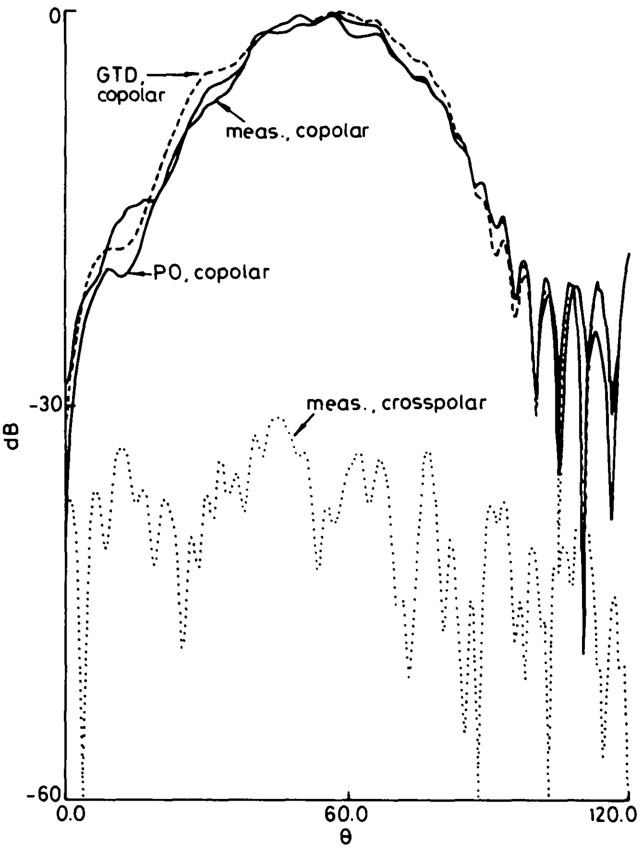

Fig. 22 *Scattered field from subreflector*
Comparison between experiment and theory

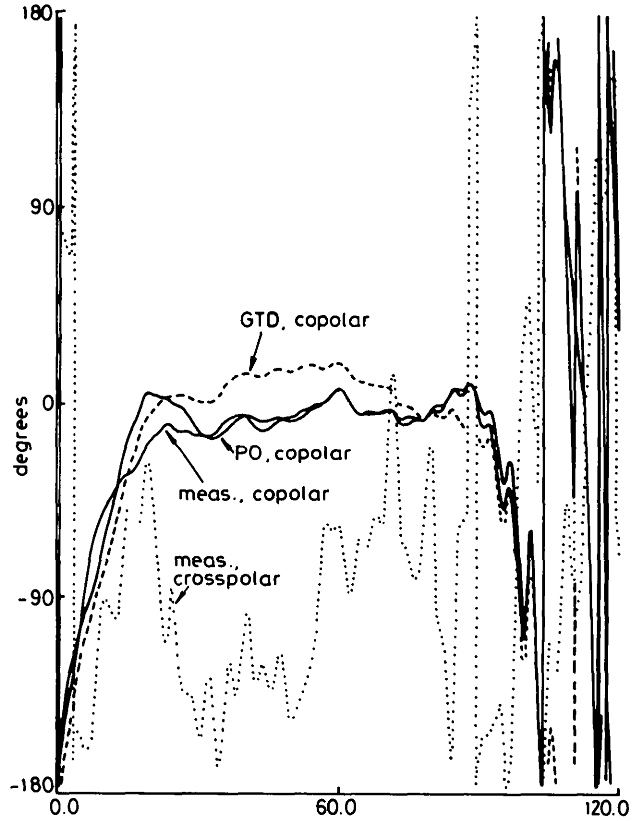

Fig. 23 *Phase of scattered field from subreflector*
Comparison between experiment and theory

6 Theory versus experiment

To confirm the accuracy of PO with near-field terms versus GTD, the configuration shown in Fig. 19 was calculated and measured. The feed is a smooth walled conical horn with semi-flare angle 15° and aperture diameter 4.9λ. The distance from the feed phase centre in the external focus of the hyperboloidal reflector to the surface is 14λ and the maximum diameter of the reflector is 15.67λ. The feed is horizontally polarised and the pattern in the symmetry plane is shown in Figs. 20 and 21. In Figs. 22 and 23 the measured, scattered field in the symmetry plane is compared with both GTD (using the model in eqn. 1) and PO (using the feed near field). It is clear from Fig. 19 that the feed will block part of the reflector, and in Figs. 22 and 23 the theoretical curves include a contribution from the field scattered by the feed. The excellent agreement between PO and experiment confirms that the copolar beam can be accurately calculated by this method.

7 Conclusion

It has been demonstrated that, if the subreflector is in the far field of the feed, both PO and GTD accurately predict the copolar beam, while only GTD is accurate with respect to the crosspolar component. If the subreflector is in the near field of the feed, PO predicts the copolar beam accurately only if the correct incident near field is used, and the crosspolar component only if corrected by PTD. In this case GTD fails, particularly with respect to copolar phase, and must be replaced by CRA.

8 References

1 ALBERTSEN, N.C., and PONTOPPIDAN, K.: 'Pattern prediction methods for high performance single and dual reflector antennas'. ESTEC Contract 3629/78/NL/AK, Ticra Report S-101-02, Ticra, Copenhagen, Denmark, 1979

2 ALBERTSEN, N.C., NIELSEN, P.H., and PONTOPPIDAN, K.: 'New concepts in multireflector antenna analysis'. ESTEC Contract 4386/80/NL/DG, Ticra Report S-137-06, Ticra, Copenhagen, Denmark, 1983

3 BURNSIDE, W.D., RUDDUCK, R.C., and MARHEFKA, R.J.: 'Summary of GTD computer codes developed at the Ohio State University', *IEEE Trans.*, 1980, **EMC-22**, pp. 238–243

4 DESCHAMPS, G.A.: 'Ray techniques in electromagnetics', *Proc. IEEE*, 1972, **60**, pp. 1022–35

5 FELSEN, L.B.: 'Complex rays', *Philips Res. Rep.*, 1975, **30**, pp. 187–95

6 FELSEN, L.B.: 'Evanescent waves', *J. Opt. Soc. Am.*, 1976, **66**, pp. 751–60

7 FELSEN, L.B.: 'Evanescent-wave tracking: new approach to the analysis of large reflector and aperture antennas', *Electron. Lett.*, 1979, **15**, pp. 531–32

8 HASSELMANN, F.V., and FELSEN, L.B.: 'Asymptotic analysis of parabolic reflector antennas', *IEEE Trans.*, 1982, **AP-30**, pp. 677–85

9 KOUYOUMJIAN, R.G., and PATHAK, P.H.: 'A uniform geometrical theory of diffraction for an edge in a perfectly conducting surface', *Proc. IEEE*, 1974, **62**, pp. 1448–61

10 LEE, S.-W., CRAMER, P. Jr., WOO, K., and RAHMAT-SAMII, Y.: 'Diffraction by an arbitrary subreflector: GTD solution', *IEEE Trans.*, 1979, **AP-27**, pp. 305–16

11 LOPEZ, A.R.: 'Ray-diffraction method for handling complex incident fields', *ibid.*, 1970, **AP-18**, pp. 821–23

12 MAUTZ, J.R., and HARRINGTON, R.F.: 'Radiation from bodies of revolution', *Appl. Sci. Res.*, 1969, **20**, pp. 405–35

13 MENTZER, C.A., and PETERS, L. Jr.: 'A GTD geometrical theory of diffraction analysis of the far-out sidelobes of Cassegrain antennas', *IEEE Trans.*, 1975, **AP-23**, pp. 702–09

14 NARASIMHAM, M.S., RAMANUJAM, P., and RAGHAVAN, K.: 'GTD analysis of near-field and far-field patterns of a parabolic subreflector illuminated by a plane wave', *ibid.*, 1981, **AP-29**, pp. 654–60

15 OHM, E.A.: 'A proposed multiple-beam microwave antenna for earth stations and satellites', *Bell Syst. Tech. J.*, 1974, **53**, pp. 1657–65

16 PONTOPPIDAN, K.: 'GTD applied to reflector antenna analysis' *in* SKWIRZYNSKI, J.K.: 'Theoretical methods for determining the interaction of electromagnetic waves with structures' (Sijthoff and Noordhoff, 1981), Chap. 7, Part 2.

17 UFIMTSEV, P.Ya.: 'The method of fringe waves in the physical theory of diffraction'. Sovjetskaye Rad Moscow, 1962

18 WANG, W.-Y., and DESCHAMPS, G.A.: 'Application of complex ray tracing to scattering problems', *Proc. IEEE*, 1974, **62**, pp. 1541–51

19 WOOD, P.J.: 'Reflector antenna analysis and design' (Peter Peregrinus Ltd., 1980)